Micro-Doppler based Human Activity Recognition using ABOA based Dual Spatial Convolution with Gated Recurrent Unit

[1]Joseph Michael Jerard V, [2]Sarojini Yarramsetti, [3]Vennira Selvi G and [4]Natteshan N V S
[1]School of Computer Science & Engineering, Presidency University, Bangalore, India.
[2]Department of Computer Science and Business Systems, Nehru Institute of Engineering and Technology, Coimbatore, Tamil Nadu, India.
[3]School of Computer Science and Engineering and Information Science, Presidency University, Bangalore, India.
[4]School of Computing, Kalasalingam Academy of Research and Education, Tamil Nadu, India.
[1]jerard.vedam@gmail.com, [3]vennira.selvi@presidencyuniversity.in, [4]natteshan@gmail.com

Correspondence should be addressed to Joseph Michael Jerard V : jerard.vedam@gmail.com.

Article Info
Journal of Machine and Computing (http://anapub.co.ke/journals/jmc/jmc.html)
Doi: https://doi.org/10.53759/7669/jmc202404042
Received 20 August 2023; Revised from 18 October 2023; Accepted 25 January 2024.
Available online 05 April 2024.

Abstract – The through-wall capability, device-free detection of radar-based human activity recognition are drawing a lot of interest from both academics and industry. The majority of radar-based systems do not yet combine signal analysis and feature extraction in the frequency domain and the time domain. Applications like smart homes, assisted living, and monitoring rely on human identification and activity recognition (HIAR). Radar has a number of advantages over other sensing modalities, such as the ability to shield users' privacy and conduct contactless sensing. The article introduces a new human tracking system that uses radar and a classifier called Dual Spatial Convolution Gated Recurrent Unit (DSC-GRU) to identify the subject and their behavior. The system follows the person and identifies the type of motion whenever it detects movement. One important feature is the integration of the GRU with the DSC unit, which allows the model to simultaneously capture the spatiotemporal dependence. Present prediction models just take into account spatial features that are immediately adjacent to each other, disregarding or just superimposing global spatial features when taking spatial correlation into account. A new dependency graph is created by calculating the correlation among nodes using the correlation coefficient; this graph represents the global spatial dependence, while the classic static graph represents the neighboring spatial dependence in the DSC unit. The DSC unit goes a step further by using a modified gated mechanism to quantify the various contributions of both local and global spatial correlation. While previous models performed worse, the suggested model outperformed them with an accuracy of 99.45 percent and a precision of 97.15 percent.

Keywords – Human Identification, Gated Recurrent Unit, Radar Based Systems, Frequency Domain, Global Spatial Dependence.

I. INTRODUCTION

The many uses of human activity recognition in fields as diverse as healthcare, surveillance, and human-computer interaction have brought it considerable attention in recent years. Assisted living, smart homes, and monitoring are just a few of the many applications that have piqued the interest in human identification and activity recognition (HIAR) [1]. Wearable and contactless modalities are two broad categories into which many have been introduced. Constantly donning and carrying around wearable sensors like ankle monitors and bracelets makes them cumbersome, prone to loss or forgetfulness, and prone to false alarms [2]. Despite these drawbacks, contactless sensing systems have attracted a lot of attention from researchers. Cameras, microphones, and radar systems are the most prevalent types of contactless sensors [3]. When it comes to lighting and blind spots, cameras aren't perfect. Ambient noise interferences can be rather noticeable to microphones [4]. On top of that, when used in residential settings, they both violate people's right to privacy. Because of its ability to preserve privacy, be resistant to light and weather, and achieve high accuracy, radar-based HIAR could be a useful addition to existing technologies [5]. According to [6], the conventional signal processing method for radar-based

HIAR depends on creating micro-Doppler signatures, extracting features, and applying classifiers such as SVM decision trees, and K-nearest neighbours.

But most research only applies one classification at a time, and that's because they only look at human identification (ID) or activity recognition [7]. An intelligent system that can identify all potential scenarios and apply the right classifier from the three integrated classifiers would be useful for practical applications. This system should be able to simultaneously apply ID and HAR if the detected scenario involves a moving target [8]. This paper presents a new way to integrate ID and HAR into a single system. There are a number of reasons why radar HAR is an exceptionally promising area for the research of robustness as compared to other fields [9]. To start, the spectrogram is the motion signature that includes all the reflected images from the human body. While still maintaining an innate sense of naturalness, perturbations in human motion can display large variability [10]. Second, the signal processing methods used to generate radar spectra have a direct bearing on their quality. Corruption can be seen in the form of system noise that is introduced during signal processing [11]. Finally, almost all radar datasets are homogeneous. Radar HAR data is typically collected in lab settings with controlled conditions, which are known for having simpler settings [12]. The diversity within these datasets is minimal, even if the data was collected over a long period of time. Therefore, models that are trained on these datasets run the danger of being overfit to features, including patterns of background noise, that might not be representative [13]. With so many high-capacity deep learning models out there, this worry stands out. To further evaluate the trained model's generalizability, robustness should be considered as an additional metric [14].

In this paper, we present a robustness analysis outline for micro-Doppler spectrogram classification errands. The main aids of this work are as shadows:

(1) One goal is to present a new HAR prediction model called DSC-GRU that takes into account the data's spatiotemporal dependence and produces more accurate predictions.
(2) The optimal weights are optimally selected by African Buffalo Optimization Algorithm (ABOA) model that improves the classification accuracy.

Thirdly, the suggested model may simultaneously incorporate data correlations based on both time and space. To do this, the GRU design incorporates a Dual Spatial Convolution (DSC) module. While the GRU is still able to learn the intricate temporal dynamics of the input, the DSC makes it easier to incorporate spatial information into its state.

The rest of the paper is prearranged as follows: **Section 2** presents the related works; **Section 3** gives the brief explanation of projected model; **Section 4** mentions the results and discussion besides lastly, the conclusion is given at **Section 5.**

II. RELATED WORKS

A method for assessing the resilience of radar micro-Doppler spectrogram categorization to corruption has been presented by Zhou et al., [15]. Common model designs are systematically examined after applying and classifying a collection of corruptions. Alternate training approaches, data augmentation, and cadence velocity diagram (CVD) transformation are also investigated. Both continuous aquatic HAR and indoor HAR are used to measure performance. Several findings are revealed by our investigation. First, because datasets are limited, relying alone on accuracy may not be sufficient to evaluate model performance. Any model that has been properly trained will be vulnerable to corruptions. Second, when it comes to accuracy and resilience, deeper CNN models are unrivalled yet, they do face the challenge of overfitting to background. Finally, while there is a small drop in accuracy, adversarial training makes systems more resistant to corruptions. Finally, a compromise between precision and resilience can be reached by merging data augmentation with adversarial training. Ultimately, our research adds to our growing body of knowledge on the intricate relationship among radar HAR tasks' model design, classification accuracy, and corruption robustness.

In their innovative system, Zhou et al. [16] simulate radar signals by converting verbal descriptions into motion data using generative models. This method greatly improves the dataset's realism and diversity, particularly for rare but important events like aberrant walking and falls. Textual descriptions enhance intraclass variety by capturing the semantic ambiguity and complexity of activities. Through the management of gait variance, adaptability to many viewpoints, and the modeling of background noise, our system increases the quality of simulations while scaling the data generation process. When real-world data samples are few, the simulated micro-Doppler dataset can help with enhance recognition. Our method makes great strides in activity identification even with small samples, greatly reducing the impact of data scarcity.

In order to enhance HAR, Guendel et al. [17] present a novel processing pipeline that takes use of multipath signals to extract useful information. A network of three radar sensors detects a moving human target engaging in continuous sequences of actions, and the pipeline separates and follows the LOS and multipath components of this target. In addition, the system has been tested with experimental data from six activities and fourteen volunteers. To do this, we compared classification metrics using neither the LOS components of the three radars in the network nor the usage of a single radar. Range-Doppler (RD) pictures obtained from the LOS and multipath components using the suggested technique may be

processed by a 12-layer convolutional neural classifier. Making use of a multiradar network's LOS and multipath components, we show that the leave-one-person-out (L1Po) test set may be significantly improved by around 11%.

Using data from the color domain, Dey et al. [18] provide a new method for fusing 2-dimensional representations of radar returns at the domain level. The convolutional mixer is an isotropic patch-based learning model that takes as input consolidated three-channel pictures formed by fusing together the individual color planes (R, G, B) of two-dimensional representations. An attentional feature level (intermediate) fusion-based convMixer model is fed the initial (domain) fused three-channel pictures. A publicly accessible dataset of radar signals of human activities is used to test the performance of the projected model. Thanks to its location-wise testing technique, which prevents data leaking, the suggested model achieves far better results than the state-of-the-art.

Using macro and micro-Doppler characteristics, Yang et al. [19] presented a lightweight multiscale neural network (TWR-FMSN) for indoor HAR. After defining the trajectories of both properties, the integrated models are used to label the trajectories at both scales for recognition in the proposed technique. In order to acquire macro-Doppler characteristics of human motion, we suggest a lightweight network that is efficient and relies on attention mechanisms. This network would use Lagrangian trajectory estimation. Furthermore, the micro-Doppler characteristics of human motion are got using a kernel-distance based micro-Doppler labeling approach. The last step in determining indoor HAR is to combine all of the retrieved micro- and macro-Doppler data. Experimental results confirm the efficacy of the suggested strategy; it may drastically cut inference time without sacrificing recognition accuracy, suggesting promising real-time deployment for practical applications.

III. PROPOSED SYSTEM

Micro-Doppler Theory

The well-known Doppler Effect occurs as an object approaches a radar sensor, altering the frequency of the reflected signals. The micro-Doppler effect is an extra modification of the primary Doppler the drive of tiny components of the subject. Specific traits, known as micro-Doppler signatures, can be produced by an object's or process's micro-Doppler effect. Considering that its many components might potentially travel in a variety of directions and at varying speeds relative to the radar. Subjects and human activities may be recognized using the target's micro-Doppler signals, which it delivers. The two-dimensional time-frequency space is the standard for displaying micro-Doppler characteristics. Due to factors including people's habits, where they stand, and the multipath effect, the spectrograms of various activities could differ from what was explained earlier. However, spectrograms of the same activity usually seem rather similar.

Data Collection

The data was collected using the radar kit. Included in the package is a TI DCA1000EVM capture card and a TI AWR1642EVM radar module. To configure the radar, start each scan, and save raw data files to the output location, you need the mmWave Studio program. The LUA Studio allows for the automation and execution of this operation in MATLAB [20]. There are three sets of data utilized in this study. The ID deep learning models are trained and validated using two datasets that are detailed in reference [21]. To train and verify the deep learning model utilized for HAR, the third dataset is utilized. Six different types of behavior make up this dataset. A total of nine human participants are utilized for each lesson. According to the summary in [20], a total of 1080 scans are obtained, with 20 scans acquired per participant every class.

The radar setup characteristics that were utilized for this project are detailed in [20], with a carrier frequency of 77 GHz. The vast bandwidth accessible in the 77 GHz range is one of its primary advantages. The bandwidth available at 77 GHz is far higher than that at 24 GHz, where the 200 MHz ISM band lies. In contrast to the two datasets, which make use of distinct sets of radar parameters, we establish a common set of parameters for all three classifiers in this study. The two ID parameters, and then used in the proposed system. This is because the radar data for each classifier is processed and sent to the deep network as RGB pictures. We use the same radar setup parameters to gather additional data for the purpose of validating the tracking algorithm. In this dataset, participants are given the option to either remain still, move freely among the six activity classifications, or do nothing at all.

.

Data Pre-Processing

When using FMCW radar, the received signals are usually transformed into a three-dimensional data cube with fast-time, channels. Applying the Fast Fourier Transform (FFT) to each dimension of the data cube changes its axes from Range to Doppler to Angle in the initial processing stage.

Classification Process: Overview

In the DSC-GRU paradigm, a GRU is housed within a DSC. Our suggested model's structure is made up of three parts: the data batch size used to model once, the length of the historical data input, and the length of the prediction data output. In addition, sampling is the process of randomly picking B-matrix blocks dimension to feed into the model during a training

epoch, after partitioning the feature matrix into many H-length matrix blocks. The geographical and temporal properties of the data are extracted using the DSG-GRU model, which is based on the existing graph structure. With the DSC-GRU model, you can still use the GRU's dynamic time series feature extraction capabilities. In order to capture the spatial properties of the input utilized to acquire the spatial topological structure network. Lastly, a fully linked layer is used to retrieve the outcomes of the output predictions.

Three points best capture the essence of the DSC-GRU: 1. A geographic correlation matrix: to discover the network's spatial correlation, build a matrix using the correlation coefficient as its basis. To improve the input network's prediction performance, a gated mechanism is utilized for spatial features fusion, which combines nearby characteristics with the input network's global features. (3) Time-related feature extraction: use a GRU network to record the input signal's temporal correlation

Spatial Dependence Modelling

The GCN classical, which developed from CNNs, has been successfully applied in several domains recently, including biochemistry, computer vision, and others, because to its exceptional capacity to manage diverse graph shapes [22].

Graph Data Definition

By projecting the network's spatial topology space, the GCN model improves the accuracy of data spatial dependencies. But as our suggested model incorporates two separate geographic scales, we must first define th The GCN model converts the network's topology Euclidean space in order to better represent the spatial linkages in the data. However, as our suggested model incorporates two different spatial structure scales, the data for the spatial structure graph must be defined independently. The relationship between neighboring nodes is described by the adjacency matrix A_a∈R^(N×N), which is obtained by mapping the adjacency graph to Euclidean space. According to the adjacency matrix, the link between the edges in set E is specified by Equation (1),

Spatial structure graph data separately. Obtaining the adjacency matrix involves mapping the adjacency graph to Euclidean space. $A_a \in R^{N\times N}$, describes the arrangement of neighbouring nodes in space. Connection relationships in the set of edges E are defined in Equation (1), as seen by the adjacency matrix.

$$A_{a_{ij}} = \begin{cases} 1(e_{ij} \in E) \\ 0(e_{ij} \notin E) \end{cases} \tag{1}$$

where $A_{a_{ij}}$ = 1 characterizes node i node j and $A_{a_{ij}}$ = 0 vice versa.

In conventional graph convolution, the adjacency matrix Aa may often only aggregate the spatial structure inside the network's nearby nodes or n-hop nodes. Ignoring the overall network topology, these simplistic graphs presume that the statuses of nodes on the same signal segment strongly impact the target node's state. Some research computed the correlation among the two-time series using the KNN method to acquire the complete network's spatial feature, allowing for a thorough exploration of the network's topological structure. From the complete network, the KNN algorithm chooses the K nodes that are most relevant to the target node based on the relevance score computed using ABO. Among the most recent meta-heuristic algorithms is the African Buffalo Optimization (ABO), first suggested by [23]. During migration, the ABO might learn to imitate the herd's effective management and communication approach. As they make decisions, they act like voters, and their movement is dictated by the majority's choice. In order to navigate and take use of their environment, they make use of two sounds: maaa and waaa. The buffalos are kept here so they may make the most of the grass and the protection they now enjoy. However, while exploring new areas, the "waaa" sound is used since the pasture at the present site might not be enough. The buffalos use these noises to their advantage in their quest for productive feeding areas. Both (2) and (3) provide mathematical expressions for this.

$$mk + 1 = mk + lp1\ (bgmax - wk) + lp2(bgmax.k - wk) \tag{2}$$

where mk denotes a “maaa” sound with a exact orientation to a buffalo k (k = 1,2,3, … n) , the best buffalo within the herd is represented by $bgmax$, while $bgmax.k$ denotes the best location which an individual buffalo k finds, $lp1$ and $lp2$ signify the limits of learning ∈ [0,1]. Through the use of (2), mk+1 shows that the buffalo has moved from its present spot mk to another spot that reflects its strong memory capacity in its migrating lifestyle. The actual adjustment of herd motion is achieved by the mathematical representation (3).

$$wk + 1 = (wk + mk)\ /ג \tag{3}$$

where wk+1 represents the migration to a new location, wk stands for the values of the current exploration, which emits the "waaa" sound, and mk is the value of existing exploitation. ג is a parameter that specifies the unit of time for the

intermission movement, and it is typically set to 1. The procedure below describes the ABO algorithm by kth buffalos randomly within the solution space. By modifying the buffalo's motion during the iterations, the final optimal outcome is achieved. During each iteration, the fitness values of each buffalo are acquired. The best global value is assigned to $bbmax$, while the best local value is assigned to $bbmax.\ k$. The buffaloes themselves keep track of where they are, and they move about following the optimal buffaloes in their immediate vicinity as determined by (2) and (3). This update allows the buffalos to move towards the optimal solution. The KNN algorithm may mistakenly identify nodes as highly linked even while they are not. A lot of data that isn't useful will be learned by the model from these nodes.

Improving the accuracy and flexibility of geographical information aggregation, the correlation coefficient R^2 is nodes. The R^2 is derived as follows:

$$SST = \sum_{k=0}^{L}\left(X_i^k - \bar{X}_i\right)^2 \tag{4}$$

$$SSR = \sum_{k=0}^{L}\left(X_j^k - \bar{X}_i\right)^2 \tag{5}$$

$$SSE = \sum_{k=0}^{L}\left(X_i^k - X_j^k\right)^2 \tag{6}$$

$$R_{ij}^2 = 1 - \frac{SSE}{SST} = \frac{SSR}{SST} \tag{7}$$

for Total, SSR for Sum of Squares Regression, and SSE for Sum of Squares Error., R_{ij}^2 stands for the degree of association between node i and node j, with values closer to 1 indicating a stronger joining, and X_i^k and $\bar{X}_i$ characterize the signal flow value and the average signal flow value k, individually. The relationship between the R^2 **Table 1** below displays the correlation coefficient and intensity of the correlation.

Table 1. The Relationship Among The R^2 Correlation Coefficient Besides Correlation Asset.

Correlation Strength	**The Value Range of R^2**
Strong	0.6 ~ 0.8
Extreme	0.8 ~ 1.0
None	R^2 < 0.2
Weak	0.2 ~ 0.4
Moderate	0.4 ~ 0.6

The correlation of road network nodes is intended based on the R_{ij}^2. It is expected that if the correlation coefficient threshold, then nodes are measured to be powerfully correlated. On this basis, Ar is distinct as Equation (8),

$$A_{r_j} = \begin{cases} 1(R_j \geq threshold) \\ 0\ (R_j < threshold) \end{cases} \tag{8}$$

where $A_{r_{ij}}$ = 1 means that the correlated and $A_{r_{ij}}$ = 0 vice versa.

Graph Data Processing

Undirected graphs based on networks are commonly utilized in prediction tasks. Here, the GCN network uses the adjacency matrix A and the weight matrix W to include the node and neighbor attributes. The following computations reveal the two-layer architecture of the GCN network:

$$GCN(A,X) = softmax\left(AReLU\left(AXW^{(0)}\right)W^{(1)}\right) \tag{9}$$

where $W^{(0)}$ besides $W^{(1)}$ are the weight media of the first and GCN network, correspondingly.

Adjacency matrix $\tilde{A}$ is clear to combine the node's own info,

$$\tilde{A} = A + \lambda I_N \tag{10}$$

where I_NThe identity matrix has dimensions equal to those of the nodes, and when the weight factor, l, has the value 1, it means that this node's information is just as essential as its neighbors'.

A symmetric normalized Laplacian matrix is used by the GCN perfect to normalize the rows and columns of the contiguousness matrix **M**.

$$A^{sys} = D^{-1/2}\tilde{A}D^{-1/2} \tag{11}$$

where the degree matrix $D \in R^{N\times N}$ is matrix, D_{ii} is the component on matrix, besides a_{ii} represents the component of the i row besides j matrix A.

$$D_{ii} = \sum_{j=1}^{N} a_{ij} \tag{12}$$

To summarize, the following equation describes the GCN network.:

$$GCN(A^{sys}, X) = softmax\left(A^{sys} ReLU\left(A^{sys} X W^{(0)}\right) W^{(1)}\right) \tag{13}$$

The topological structural information merged by substituting the adjacent matrix Aa besides correlation matrix Ar matrix A in the conventional GCN network.

Dual Spatial Convolution

The procedure of incorporating the structural details of the nearby space and the world space, respectively. The significance of the neighboring and global data sets is presumed to be equal if they are just overlay. On the other hand, when it comes to making predictions, it's not feasible to artificially determine how important nearby and worldwide data is. Performing even a basic superposition will significantly lower the model's prediction accuracy. In order to improve the prediction accuracy, the gated mechanism learns the weight matrix and adjusts the significance of both local besides global info to the target node.

The estimated R2 correlation also goes over the threshold, which is a special instance. When global information is integrated, the data of those neighboring nodes will likewise be fused. At least partially, it solves the issue where the standard graph convolution model fails to take into account the fact that various neighbors have varied impacts on the target node. The operation for G_{a} and G_{r} is recorded as Equations (14)–(17):

$$GCN_a = softmax\left(A_a^{sys} ReLU\left(A_a^{sys} X W_a^{(0)}\right) W_a^{(1)}\right) \tag{14}$$

$$GCN_r = softmax\left(A_r^{sys} ReLU\left(A_r^{sys} X W_r^{(0)}\right) W_r^{(1)}\right) \tag{15}$$

$$Fusion = \sigma(W_o.(GCN_a + GCN_r) + b_o) \tag{16}$$

$$Output = GCN_a * (1 - Fusion) + GCN_r * Fusion \tag{17}$$

in which the parameter matrices W and b are located, Fusion takes into account both local and global spatial information, whereas Output is the DSC unit's output. To change the relative weight of the global data, fusion is employed. The greater the significance of the worldwide info, the closer it is to 1. Next, while making predictions, greater emphasis is placed on the spatial information of the entire road network, and vice versa, on the nearby region. In conclusion, the DSC to achieve a balance in the relative significance connection between the global space and the nearby universe. Because of this, the DSC is able to better capture the spatial dependency of data and extract the urban road network.

Spatiotemporal Dependence Modeling

We extracted the data's spatial dependency using the DSC in the preceding part. Still, getting features from time series is a major challenge in the prediction process. The RNN is the go-to tool for handling time series data, and it shows promise on a variety of models. Traditional RNNs are unable to extract the time-dependent characteristics from traffic flow data because of the flaws of gradient expansion and gradient disappearance. As alternatives to RNNs, the LSTM and GRU have been suggested. They address the issues mentioned above. The GRU and the LSTM both work on similar concepts. Similar to RNNs, both use a gating mechanism and cells to address the issue of reliance on time series over the long run.

With fewer parameters and less computing power required, GRUs are easier to train and converge than LSTMs, and thus pose less of a danger of overfitting. Hence, this article models the spatiotemporal dependency using the GRU framework. By incorporating the DSC into the GRU framework, a suggested prediction model called the DSC-GRU may acquire data that is reliant on both time and space.

The forward propagation of the DSC-GRU perfect is expressed by Equations (18)–(21).

$$r_t = \sigma(W_r.[X_r, H_{t-1}] + b_r) \tag{18}$$

$$u_t = \sigma(W_u.[X_r, H_{t-1}] + b_u) \tag{19}$$

$$c_t = tanh(W_c.DSC([X_t, (r_t * H_{t-1})]) + b_c) \tag{20}$$

$$H_t = u_t * H_{t-1} + (1 - u_t) * c_t \tag{21}$$

where W, b is the training process's limit matrix for each state, s(·) is defined in the previous section, tanh(·) maps the input to the [−1, 1] intermission to avoid gradient explosion caused by the backpropagation process's large sum of parameters, and DSC(·) is the result from the DSC cell control.

As it processes the input Xt at time t and the GRU model maintains the GRU representation's capacity to capture the time series' long-term dependency. In this case, the temporal data from the past is mixed with the data from the present. The time series' inherent dynamic characteristics are preserved. In light of this, the DSC unit is connected to document the

space-dependent traffic statistics. The future instant gets the legitimate part of the spatiotemporal data received in the past through reset gates.

At instant t, the DSC-GRU model's input hidden layer state already includes spatial and temporal data from the moment before. The DSC takes as input the present instant and merges it with authentic spatiotemporal data from the past. One aspect is the merging of the spatial characteristics of the present input data. Conversely, geographical details in historical records are more important. So far, the DSC embedding has enhanced the GRU model by adding network spatial information to every state. In the same way that the GRU model transmits temporal information from one time step to another, it also transmits geographical information. The aforementioned step is iterated upon several times during forward propagation to bolster the DSC's learning of spatial characteristics and enhance the representation's capacity to extract spatial relationships. To review, the DSC-GRU model is able to uncover the data's latent spatial and temporal dependencies. Among other things, the DSC unit may be utilized to ascertain the overall network's topology and, from there, the data's spatial reliance. Another thing is that the GRU model takes into account the long-term temporal relationship in data in order to get the data's temporal dependency. The prediction work is now finished.

IV. RESULTS AND DISCUSSION

The Intel Core i7-11800H CPU, NVIDIA GeForce the Deep MATLAB 2021b are utilized to execute this application. Training all three classifiers using the given capabilities takes a total of twenty-four minutes. We implemented a sensor network using two BumbleBee radars [24]. At 5.8 GHz, the Bumblebee radar—a low-power Pulse Doppler radar—runs its show. The range it can cover is up to ten meters. The price of a single BumbleBee radar is less than $100. It can run on 1.5v alkaline capacity of 2400 mAh for approximately 8 days at full duty cycle, thanks to its 12 mAh consumption. **Table 2** displays the primary characteristics of the BumbleBee radar. It is common practice to use a TelosB mote with a BumbleBee radar. With its support for IEEE 802.15.4, the TelosB mote enables low-power wireless communication. It runs on TinyOS, an open-source OS that facilitates massive, autonomous sensor networks.

"Node 1" and "Node 2" are the two nodes that make up the sensor network, which also includes a single base station. A BumbleBee radar and a TelsoB mote are contained in each node. A TelosB mote sends station via ZigBee from a BumbleBee laptop, which serves as the base station. After the sensor nodes gather radar signals, it analyzes and receives them. To avoid Line-of-Sight obstacles and get additional data about the things being studied, scan an indoor space from two separate angles. Remember that our radar sensor network may be expanded if needed. This network may easily accommodate more nodes that are wirelessly linked.

Table 2. Bumblebee Radar Specifications

Onboard antenna	**Antenna**
I & Q channels	Coherent output
2.6 cm/s to 2.6 m/s	Responds to radial velocity
60-degree conical coverage pattern	Coverage pattern
Up to 10m	Detection range
0.2m	Range gate sharpness
About 12 mA	Total power draw

Validation Analysis of Projected Model

Table 3 shows the results of comparation the proposed model to current approaches using various metrics in an experimental setting.

Table 3. Experimental analysis of Proposed Model

Methods	**Accuracy**	**Precision**	**Recall**	**F-score**
DBN	91.20	92.48	91.26	91.49
CNN	91.40	91.69	91.82	91.20
RNN	90.95	90.39	90.32	90.25
LSTM	93.19	94.32	93.15	93.96
BLSTM	90.82	90.82	90.92	90.46
GRU	97.50	96.15	95.13	95.15
DSC-ABOA-GRU	99.45	97.15	96.89	96.99

In **Table 3** represent that the Experimental analysis of Proposed Model. In the analysis of DBN perfect reach the accuracy as 91.20 and precision as 92.48 and recall as 91.26 and F-score as 91.49 similarly. Then the CNN perfect reach

the accuracy as 91.40 and precision as 91.69 and recall as 91.82 and F-score as 91.20 similarly. Then the RNN perfect reach the accuracy as 90.95 and precision as 90.39 and recall as 90.32 and F-score as 90.25 similarly. Then the LSTM perfect reach the accuracy as 93.19 and precision as 94.32 and recall as 93.15 and F-score as 93.96 similarly. Then the BLSTM perfect reach the accuracy as 90.82 and precision as 90.82 and recall as 90.92 and F-score as 90.46 similarly. Then the GRU perfect reach the accuracy as 97.50 and precision as 96.15 and recall as 95.13 and F-score as 95.15 similarly. Then the DSC-ABOA-GRU perfect reach the accuracy as 99.45 and precision as 97.15 and recall as 96.89 and F-score as 96.99 similarly. **Fig 1** shows the visual representation of proposed deep learning classifier and **Fig 2** shows the graphical description of different models for HAR recognition.

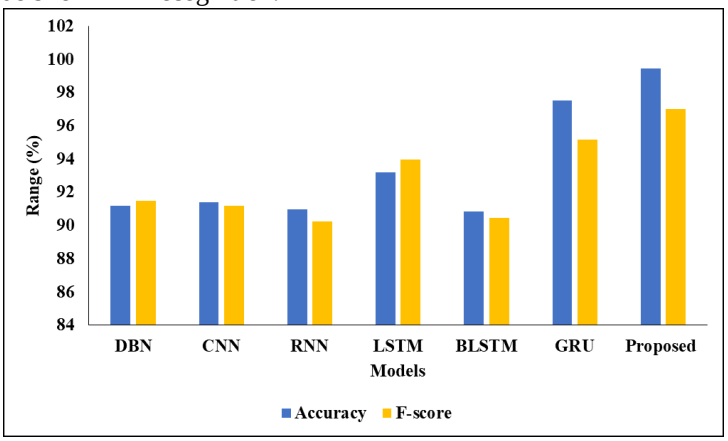

Fig 1. Visual Representation of Proposed Deep Learning Classifier.

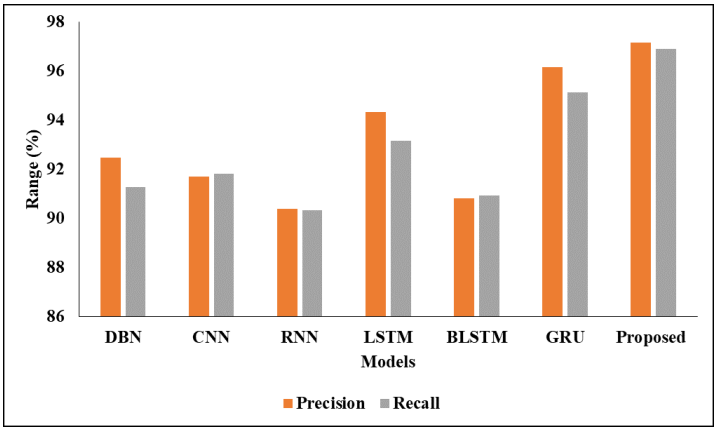

Fig 2. Graphical Description of different models for HAR Recognition.

V. CONCLUSION

This work presents a radar-based human tracking system that can determine the type of motion shown by a single individual in order to construct an autonomous stage that can use ID and HAR in practical scenarios. We use DSC-GRU classifiers to identify the person and their behavior based on the motion type that we notice. Two radar datasets are created to retrain and networks used in the proposed model's construction, which is based on deep transfer learning. One usage of the DSC unit is to describe the data's spatial dependency and capture the network space's topological structure. When training, DSC takes into account both the local and global properties of nodes throughout the space, using the correlation matrix, in contrast to conventional graph convolutional networks. The purpose of implementing the gated instrument is to regulate the value-relationship between local and global data. The effects of the network's geographic dependency are thoroughly examined. A GRU, on the other hand, can describe data's reliance on time and capture the features of dynamic vicissitudes in data flow. Each GRU state now has additional geographic data thanks to the DSC unit, which is integrated into the GRU network. As an alternative, the suggested classifier used a deep network that was trained and validated by a variety of people to categorize various behaviors. Sensitive storage facilities, where only authorized staff are permitted to do specific tasks (such as retrieving goods or moving carts), might be a potential use case for this idea. In addition, the radar-based system is designed to withstand light and weather conditions, making it ideal for use in challenging outdoor settings where vision-based systems may not be as effective. To take advantage of irregular motion scenarios besides increase the sum of identifiable objects per dimension, future research can include data fusion algorithms to integrate radar data for a more comprehensive picture of the target area.

Data Availability
No data was used to support this study.

Conflicts of Interests
The author(s) declare(s) that they have no conflicts of interest.

Funding
No funding agency is associated with this research.

Competing Interests
There are no competing interests.

References

[1]. L. Qu, Y. Wang, T. Yang, and Y. Sun, "Human Activity Recognition Based on WRGAN-GP-Synthesized Micro-Doppler Spectrograms," IEEE Sensors Journal, vol. 22, no. 9, pp. 8960–8973, May 2022, doi: 10.1109/jsen.2022.3164152.
[2]. M. M. Rahman, S. Z. Gurbuz, and M. G. Amin, "Physics-Aware Generative Adversarial Networks for Radar-Based Human Activity Recognition," IEEE Transactions on Aerospace and Electronic Systems, vol. 59, no. 3, pp. 2994–3008, Jun. 2023, doi: 10.1109/taes.2022.3221023.
[3]. M. Chakraborty, H. C. Kumawat, S. V. Dhavale, and A. A. B. Raj, "DIAT-μ RadHAR (Micro-Doppler Signature Dataset) & μ RadNet (A Lightweight DCNN)—For Human Suspicious Activity Recognition," IEEE Sensors Journal, vol. 22, no. 7, pp. 6851–6858, Apr. 2022, doi: 10.1109/jsen.2022.3151943.
[4]. F. Aziz, O. Metwally, P. Weller, U. Schneider, and M. F. Huber, "A MIMO Radar-Based Metric Learning Approach for Activity Recognition," 2022 IEEE Radar Conference (RadarConf22), Mar. 2022, doi: 10.1109/radarconf2248738.2022.9764202.
[5]. R. Mazzieri, J. Pegoraro and M. Rossi, "Enhanced Attention-Based Unrolling for Sparse Sequential micro-Doppler Reconstruction," 2023, arXiv preprint arXiv:2306.14233.
[6]. S. Yang et al., "The Human Activity Radar Challenge: Benchmarking Based on the 'Radar Signatures of Human Activities' Dataset From Glasgow University," IEEE Journal of Biomedical and Health Informatics, vol. 27, no. 4, pp. 1813–1824, Apr. 2023, doi: 10.1109/jbhi.2023.3240895.
[7]. Y. Zhao, A. Yarovoy, and F. Fioranelli, "Angle-Insensitive Human Motion and Posture Recognition Based on 4D Imaging Radar and Deep Learning Classifiers," IEEE Sensors Journal, vol. 22, no. 12, pp. 12173–12182, Jun. 2022, doi: 10.1109/jsen.2022.3175618.
[8]. F. J. Abdu, Y. Zhang, and Z. Deng, "Activity Classification Based on Feature Fusion of FMCW Radar Human Motion Micro-Doppler Signatures," IEEE Sensors Journal, vol. 22, no. 9, pp. 8648–8662, May 2022, doi: 10.1109/jsen.2022.3156762.
[9]. X. Feng et al., "Millimeter-Wave Radar Monitoring for Elder's Fall Based on Multi-View Parameter Fusion Estimation and Recognition," Remote Sensing, vol. 15, no. 8, p. 2101, Apr. 2023, doi: 10.3390/rs15082101.
[10]. M. Chakraborty, H. C. Kumawat, S. V. Dhavale, and A. B. Raj A., "DIAT-RadHARNet: A Lightweight DCNN for Radar Based Classification of Human Suspicious Activities," IEEE Transactions on Instrumentation and Measurement, vol. 71, pp. 1–10, 2022, doi: 10.1109/tim.2022.3154832.
[11]. J. Pegoraro, J. O. Lacruz, M. Rossi, and J. Widmer, "SPARCS: A Sparse Recovery Approach for Integrated Communication and Human Sensing in mmWave Systems," 2022 21st ACM/IEEE International Conference on Information Processing in Sensor Networks (IPSN), May 2022, doi: 10.1109/ipsn54338.2022.00014.
[12]. Y. Ding, R. Liu, Y. She, B. Jin, and Y. Peng, "Micro-Doppler Trajectory Estimation of Human Movers by Viterbi–Hough Joint Algorithm," IEEE Transactions on Geoscience and Remote Sensing, vol. 60, pp. 1–11, 2022, doi: 10.1109/tgrs.2022.3171208.
[13]. X. Qiao, Y. Feng, T. Shan, and R. Tao, "Person Identification With Low Training Sample Based on Micro-Doppler Signatures Separation," IEEE Sensors Journal, vol. 22, no. 9, pp. 8846–8857, May 2022, doi: 10.1109/jsen.2022.3162590.
[14]. S. Abadpour et al., "Angular Resolved RCS and Doppler Analysis of Human Body Parts in Motion," IEEE Transactions on Microwave Theory and Techniques, vol. 71, no. 4, pp. 1761–1771, Apr. 2023, doi: 10.1109/tmtt.2022.3218304.
[15]. Y. Zhou, X. Yu, M. Lopez-Benitez, L. Yu, and Y. Yue, "Corruption Robustness Analysis of Radar Micro-Doppler Classification for Human Activity Recognition," Jan. 2024, doi: 10.36227/techrxiv.24591924.v2.
[16]. Y. Zhou, M. López-Benítez, L. Yu, and Y. Yue, "Text2Doppler: Generating Radar Micro-Doppler Signatures for Human Activity Recognition via Textual Descriptions," Mar. 2024, doi: 10.36227/techrxiv.171073563.32444449/v1.
[17]. R. G. Guendel, N. C. Kruse, F. Fioranelli, and A. Yarovoy, "Multipath Exploitation for Human Activity Recognition Using a Radar Network," IEEE Transactions on Geoscience and Remote Sensing, vol. 62, pp. 1–13, 2024, doi: 10.1109/tgrs.2024.3363631.
[18]. A. Dey, S. Rajan, G. Xiao, and J. Lu, "Radar-Based Human Activity Recognition Using Multidomain Multilevel Fused Patch-Based Learning," IEEE Transactions on Instrumentation and Measurement, vol. 73, pp. 1–14, 2024, doi: 10.1109/tim.2024.3374286.
[19]. X. Yang, W. Gao, X. Qu, P. Yin, H. Meng, and A. E. Fathy, "A Lightweight Multiscale Neural Network for Indoor Human Activity Recognition Based on Macro and Micro-Doppler Features," IEEE Internet of Things Journal, vol. 10, no. 24, pp. 21836–21854, Dec. 2023, doi: 10.1109/jiot.2023.3301519.
[20]. A. Alkasimi, A. Pham, C. Gardner, and B. Funsten, "Geolocation tracking for human identification and activity recognition using radar deep transfer learning," IET Radar, Sonar & Navigation, vol. 17, no. 6, pp. 955–966, Mar. 2023, doi: 10.1049/rsn2.12390.
[21]. A. Alkasimi et al., "Dual-Biometric Human Identification Using Radar Deep Transfer Learning," Sensors, vol. 22, no. 15, p. 5782, Aug. 2022, doi: 10.3390/s22155782.
[22]. A. Thirumalraj, V. S. Anusuya, and B. Manjunatha, "Detection of Ephemeral Sand River Flow Using Hybrid Sandpiper Optimization-Based CNN Model," Advances in Civil and Industrial Engineering, pp. 195–214, Nov. 2023, doi: 10.4018/979-8-3693-1194-3.ch010.
[23]. J. B. Odili and J. O. Fatokun, "The Mathematical Model, Implementation and the Parameter-Tuning of the African Buffalo Optimization Algorithm," 2020 International Conference in Mathematics, Computer Engineering and Computer Science (ICMCECS), Mar. 2020, doi: 10.1109/icmcecs47690.2020.240886.
[24]. F. Luo, E. Bodanese, S. Khan, and K. Wu, "Spectro-Temporal Modeling for Human Activity Recognition Using a Radar Sensor Network," IEEE Transactions on Geoscience and Remote Sensing, vol. 61, pp. 1–13, 2023, doi: 10.1109/tgrs.2023.3270365.